

Calibrating Inverted Echo Sounders Equipped with Pressure Sensors

CHRISTOPHER S. MEINEN AND D. RANDOLPH WATTS

Graduate School of Oceanography, University of Rhode Island, Narragansett, Rhode Island

(Manuscript received 24 July 1997, in final form 13 November 1997)

ABSTRACT

The addition of an accurate pressure sensor to the inverted echo sounder (IES) has allowed for the development of a new method for calibrating the IES's acoustic travel-time record without the need for coincident conductivity–temperature–depth (CTD) or expendable bathythermograph profiles. Using this method, the round-trip travel-time measurement of the IES can be calibrated into various dynamic quantities with better accuracy than was possible with previous methods. For a set of four IES records from the Newfoundland Basin, the estimate of the accuracy of the geopotential height anomaly (integrated between 100 and 4000 db) calibrated from the IES measurements was reduced from 0.65 to 0.52 $\text{m}^2 \text{s}^{-2}$, which is a substantial reduction toward the intrinsic scatter of the geopotential height anomaly versus travel-time relationship for this region (0.42 $\text{m}^2 \text{s}^{-2}$). The addition of the pressure sensor to the IES results in reduced errors and eliminates the need for coincident CTD measurements. Moreover, the pressure sensor provides a complementary dataset recording the changes of the barotropic pressure field.

1. Introduction

An inverted echo sounder (IES) is an ocean-bottom instrument that measures the time for a 10-kHz sound pulse to travel round-trip to the ocean surface and back (Watts and Rossby 1977; Chaplin and Watts 1984). In use since the mid-1970s, these instruments provide up to two-year-long hourly time series of acoustic travel time τ . The τ measurements can be used to estimate the depth of isothermal surfaces in the main thermocline, the geopotential height anomaly between two pressure levels, or other dynamic and descriptive quantities (Rossby 1969; Watts and Johns 1982; He et al. 1997). Historical hydrography can be used to determine the empirical relationship between these quantities for a given region. Coincident measurements from a conductivity–temperature–depth (CTD) probe or an expendable bathythermograph (XBT) have been used to calibrate these relationships from τ (usually just determining an additive constant); effectively, this calibration is required to determine the precise depth of each instrument.

Although some IESs in earlier experiments have been equipped with pressure gauges (PIES), the τ and bottom pressure P records were calibrated and used independently. In particular, Watts and Kontoyiannis (1990) used the pressure measurements to test the drift and accuracy of the pressure sensors, and Shay et al. (1995)

and Watts et al. (1995) used the pressure measurements to study deep geostrophic flows. This paper presents a new method of using P measurements to calibrate the measured acoustic travel times τ . The pressure measurement provides the instrument depth with improved accuracy. The new calibration, therefore, provides improved accuracy for the dynamic variables that can be estimated from the τ measurement, as will be shown.

2. Simulating an IES using historical hydrographic data

Examples of the functional relationships between acoustic travel time and various standard dynamic variables may be found in Watts and Rossby (1977) (Sargasso Sea), Watts and Johns (1982) (Gulf Stream), Chiswell et al. (1986) (eastern equatorial Pacific), Hallock (1987) (Gulf Stream and Sargasso Sea), Trivers and Wimbush (1994) (North Atlantic), James and Wimbush (1995) (North Pacific and Kuroshio Current), Garzoli and Bianchi (1987) (Malvinas and Brazil Currents), Garzoli and Gordon (1996) (Benguela Current), and Chiswell (1994) (Hawaii).

These papers have used a number of different methods to represent the vertical integral of acoustic travel time. The common goal among them is to simulate (from historical hydrographic data) an IES that measures temporal variations while moored at a fixed (x, y, z) point [where z represents absolute height, not depth measured below the sea surface, whose height itself varies with (x, y, t)]. Common to all of these simulations is the assumption that temporal variations at one site due to

Corresponding author address: D. Randolph Watts, Graduate School of Oceanography, University of Rhode Island, South Ferry Road, Narragansett, RI 02882.
E-mail: randy@drw.gso.uri.edu

mesoscale eddy variability may be simulated from the combined (x, y, t) variations among a set of hydrographic profiles for the region. The need then is, on the one hand, to select from a space-time region data that are limited enough to exclude variability that would occur only “away” from the desired (x, y) site and, on the other hand, to select enough data to include and represent the full range of variability that can occur at the site (Hallock 1987; Trivers and Wimbush 1990; James and Wimbush 1995).

The choice of integration variable (z or P), and in particular the specification of integration limits, also differs among the aforementioned authors. This paper will not review the different approaches. The common goal is to represent the round-trip vertical integral of acoustic travel time to a fixed height z in the ocean. This is represented mathematically as

$$\tau_{\text{sim}} = 2 \int_0^{P_{\text{sim}}} \frac{1}{\rho g c} dP', \quad (1)$$

where ρ , g , c , and P are the density, gravity, sound speed, and pressure, respectively. The choice to integrate between constant pressure limits is motivated by the following argument. First, bear in mind that the ocean surface height η may change with steric height and with atmospheric pressure change and ocean barotropic pressure change, but hydrography can determine only the steric height changes. An alternative choice for the τ integral would be to integrate the hydrographic profiles with height z between the surface η and a fixed distance below the sea surface. However, because of these substantial variations in η , this is not as good a representation of a fixed height. A typical range of variation in the absolute height is approximately 1 m. On the other hand, it has been observed in the deep ocean that the bottom pressures and the surface atmospheric pressures vary independently, each by about 0.3 db (Qian and Watts 1992), which corresponds to approximately 0.3 m of hydrostatic height changes. Hence, the τ representation in Eq. (1) is preferable because it more nearly represents a constant absolute height than an integration between z limits.

Another subtle detail is important in the practical application of Eq. (1) to a regional dataset. The gravitational acceleration g depends upon latitude. Hence, for the *same* profile of salinity and temperature occurring at *different* latitudes, the (P, z) relation would differ (by more than 1 db per 5° of latitude at 3500 db). The approach taken here is to select a target latitude, ϕ_t , and stretch or shrink the P axis from that that it has at the observed latitude, ϕ_o , to match that of the target latitude. This is done by using the algorithm of Fofonoff and Millard (1983) to convert the pressures from the hydrographic cast into depths, where $g = g_o(\phi_o, z)$ is calculated using the observed latitude ϕ_o . The algorithm of Fofonoff and Millard is then inverted, and the depths are converted back into pressures, P_t . For this second

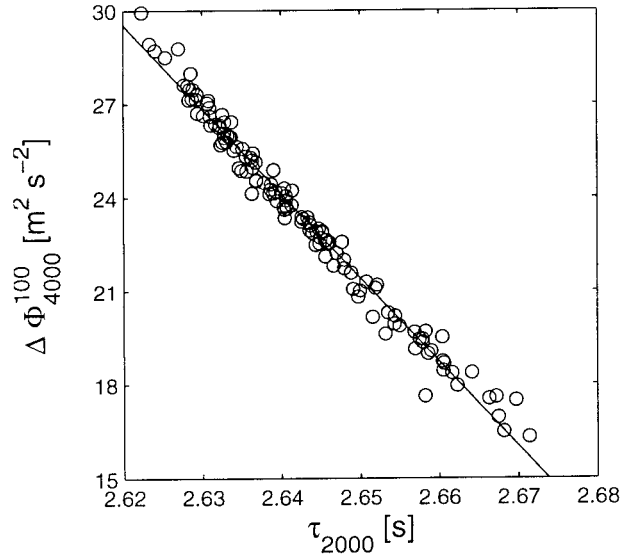


FIG. 1. Plot of geopotential height anomaly integrated between 100 and 4000 db vs the acoustic travel time τ_{sim} integrated between the surface and 2000 db. Quantities were determined from about 130 CTD casts in the Newfoundland Basin near 42°N during 1993–95. The standard deviation about the fitted line is $0.42 \text{ m}^2 \text{ s}^{-2}$.

calculation, however, $g = g_t(\phi_t, z)$ is determined using the target latitude ϕ_t . This procedure is repeated for all of the hydrographic casts to be used from the region. In this manner, the latitudinal dependence of the pressure range of integration is removed, leaving the integration range as close to constant as possible, and the simulation of the IES is at a fixed latitude. For example, if $P_{\text{sim}} = 2000$ db, we denote

$$\tau_{2000} = 2 \int_0^{2000} \frac{1}{\rho' g_t c'} dP',$$

with ρ' and c' designating profiles as a function of P_t . (Note that deeper bottom pressures than 2000 db are simulated later; this calibration method is applicable to the full depth of any IES.)¹

For the purpose of providing an example to compare the new calibration method using the measurement of bottom pressure to the traditional method for calibrating an IES, this paper will focus on the relationship between the geopotential height anomaly, integrated between 100 and 4000 db and τ_{2000} . The geopotential height anomaly is determined from the same hydrography via

$$\Delta\Phi_{4000}^{100} = \int_{100}^{4000} \delta dP', \quad (2)$$

¹ An alternative method, which we had adopted after this paper went to press, is to perform the τ_{sim} and τ_{2000} integrals from CTD data using a constant $g = 9.8 \text{ m s}^{-2}$. Then to calibrate the PIES at a given latitude and depth, one must only accurately account for the ratio of its site-specific $g(\phi, z)$ to 9.8 m s^{-2} .

where δ represents the specific volume anomaly as a function of $P = P_i$. Figure 1 shows $\Delta\Phi_{4000}^{100}$ plotted against τ_{2000} , calculated from Eqs. (2) and (1) using about 130 hydrographic casts from the Newfoundland Basin near 42°N. The relationship between these quantities could be represented by a polynomial; it is adequate for our purpose of demonstrating the improved accuracy of the pressure method of calibration to approximate this relationship as linear (shown in Fig. 1 as a solid line):

$$\Delta\Phi_{4000}^{100} = A \times \tau_{2000} + B, \quad (3)$$

where $A \approx -270 \text{ m}^2 \text{ s}^{-3}$ and $B \approx 737 \text{ m}^2 \text{ s}^{-2}$. If an IES in the Newfoundland Basin region was moored at a depth of precisely 2000 db, the slope and intercept values derived from this simulation could be directly applied to the time series of τ_{2000} measurements to obtain a time series of $\Delta\Phi_{4000}^{100}$. Unfortunately, the depth of the IES in steep topography might not be known by bathymetric survey to an accuracy of better than $\pm 30 \text{ m}$, which would result in a travel-time bias of 40+ ms. Since the entire signal of a major current like the North Atlantic Current or the Gulf Stream is 40–50 ms, such a bias must be avoided by using an alternative calibration method, such as the following.

3. Calibration of the IES

The traditional method of calibrating the IES assumes that the slope A in Eq. (3) is not dependent on the pressure at which τ is simulated, so long as P_{sim} is far below the main pycnocline. Rather, the depth dependence of τ is solely absorbed by changing the intercept B to B' . Under this assumption, all that is required to determine $\Delta\Phi_{4000}^{100}$ is to determine the appropriate B' for each IES site.

The method that has commonly been used for determining the intercept B' is to use information from one or more coincident CTDs. Equation (3) is rearranged to give

$$B' = \Delta\Phi_{4000}^{100} - A \times \tau_{\text{meas}}, \quad (4)$$

where τ_{meas} is the travel time measured by the IES at its actual bottom pressure P_{ies} and $\Delta\Phi_{4000}^{100}$ is the geopotential height anomaly integrated from the coincident CTD. The resulting intercept B' is valid at P_{ies} . Multiple CTD drops at the IES site during the period of the deployment allow for multiple estimates of B' , and averaging these produces a “best” estimate for B' (Tracey et al. 1997).

The final calibrated values of $\Delta\Phi_{4000}^{100}$ using this method are subject to two kinds of errors: biases due to errors in the determination of B' and random scatter. The two sources of random scatter are 1) the errors in the τ_{meas} record after 40-h low-pass filtering [$(\text{rms scatter of hourly measurements})/\sqrt{\text{degrees of freedom}} = 1 \text{ ms}/\sqrt{40} = 0.15 \text{ ms}$ that corresponds to $\epsilon_a = 0.045 \text{ m}^2 \text{ s}^{-2}$], which propagate through Eq. (3) to be errors in $\Delta\Phi_{4000}^{100}$; and 2) the scatter of the fit of Eq. (3) (see Fig. 1, $\epsilon_b = 0.42$

$\text{m}^2 \text{ s}^{-2}$). Errors in the determination of B' result in biases for the time series of $\Delta\Phi_{4000}^{100}$. There are three sources of error in the determination of B' : 1) the error in the hourly τ_{meas} [1 ms (Chaplin and Watts 1984) that corresponds to $\epsilon_c = 0.27 \text{ m}^2 \text{ s}^{-2}$] at the time of the coincident CTD, which affects the determination of B' via Eq. (4); 2) the scatter introduced because τ_{meas} in Eq. (4) represents an integration over the full water column, while the integration of $\Delta\Phi_{4000}^{100}$ from the coincident CTD measurements is affected only by variability in the range of integration between 100 and 4000 db ($\epsilon_d = 0.14 \text{ m}^2 \text{ s}^{-2}$ based on the observed variability in density structure below 4000 db for this region); and 3) due to the spatial offset between the CTD and the IES sites ($0.27 \text{ m}^2 \text{ s}^{-2}$ per kilometer distance between the CTD and IES sites based on the maximum observed change in geopotential height anomaly across the front). The spatial offset error introduces a random scatter due to the deflections of isotherms by internal waves during the several hours involved in the CTD measurement as well as a bias due to the ambient horizontal gradient of the main thermocline depth. Note that when multiple CTDs are taken at a site, ϵ_c , ϵ_d , and ϵ_e are reduced by a factor of \sqrt{N} , where N is the number of CTD casts. An estimate of the total rms error in this traditional method, denoted ϵ_{tm} , is given by

$$\epsilon_{\text{tm}} = \left[(\epsilon_a)^2 + (\epsilon_b)^2 + \left(\frac{\epsilon_c}{\sqrt{2}} \right)^2 + \left(\frac{\epsilon_d}{\sqrt{2}} \right)^2 + \left(\frac{2.5 \times \epsilon_e}{\sqrt{2}} \right)^2 \right]^{1/2} \\ = 0.65 \text{ m}^2 \text{ s}^{-2}$$

when the concurrent CTDs were taken 2.5 km from the IES site, and two CTDs were taken at the site during the record.

4. Calibrating a PIES

The inclusion of pressure sensors on the PIES provides an alternative calibration method. ParoScientific, Inc., the manufacturer of the pressure sensors used in the PIES, states in its technical brochures an absolute pressure accuracy of 0.01% of full scale, or 0.5 db, in up to 5000-m depth. The accuracy of the pressure sensors has also been tested by predicting the bottom pressure of the PIES using the measured travel times and a sound-speed profile based on coincident full-water-column CTDs. For 11 PIES in three different experiments the resulting mean offset between the predicted pressure and the measured pressure was about 1 db, about half of which may be attributable to errors in the sound-speed algorithm rather than the pressure sensor (Meinen and Watts 1997). Thus, the pressure sensor provides the accurate depth information required to calibrate an IES τ record. Calibration for an individual PIES using this new method consists only of using the historical hydrography to simulate IESs, where $P_{\text{sim}} = P_{\text{ies}}$ in Eq. (1), and then the A and B in Eq. (3) will apply directly to the measured travel times (rather than a 2000-db sim-

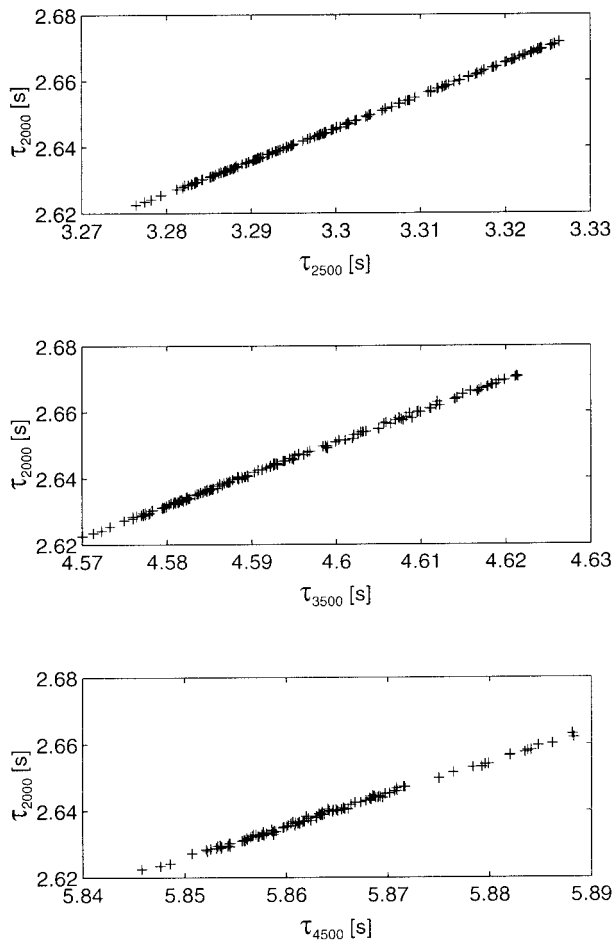


FIG. 2. Comparison of the round-trip travel time τ_{sim} at 2000 db to τ_{sim} at 2500, 3500, and 4500 db as labeled on the x axis. Units are seconds.

ulation). Also note that this calibration requires that we account for three well-known constant offsets intrinsic to the measurements used in this study. A discussion of these offsets is given in appendix A.

For a deployment involving multiple PIES, the method described above has the weakness that it would require determining a set of coefficients A and B for each individual PIES since no two instruments would be at exactly the same pressure. If these PIES were being calibrated into not only $\Delta\Phi_{4000}^{100}$ but also heat content and potential energy anomaly, for example, this would be cumbersome. It might also lead to inconsistencies between different IESs due to small errors in fitting the coefficients, especially for variables for which it is necessary to fit a nonlinear function.

A better approach is for the travel-time measurements from different sites to be projected onto a common (deep) pressure level, P_{com} , using $\tau_{\text{com}} = \mathcal{A} \times \tau_{\text{meas}} + \mathcal{B}$ (note script \mathcal{A} , \mathcal{B} differ from A , B). This approach requires only a single set of coefficients for other dynamic variables to be estimated from the τ_{com} measurements.

Using historical hydrography to simulate IESs at various pressures, it can be shown that $\tau_{\text{sim}1}$ at any pressure level, P_1 , which is significantly below the thermocline, is linearly related to $\tau_{\text{sim}2}$ at any other deep pressure level, P_2 . Figure 2 shows a number of examples. The slopes are very nearly but not exactly 1. By studying a number of these relations it has been determined that the slope and intercept of the linear relationships between τ_{sim} at different pressures are simple functions of pressure themselves, $\mathcal{A}(P)$ and $\mathcal{B}(P)$. Appendix B presents the details of the conversion of the measured τ_{meas} at P_{ies} into τ_{com} on a common pressure level, P_{com} , which we take to be 2000 db in this study. This allows the use of a single set of A and B coefficients in Eq. (3) derived from a simulation of IESs at P_{com} .

This pressure calibration also is subject to bias and random errors. The two sources of random scatter are the same as for the traditional method: 1) the errors in the τ_{meas} record after 40-h low-pass filtering [$(\text{rms scatter of hourly measurements})/\sqrt{\text{degrees of freedom}} = 1 \text{ ms}/\sqrt{40} = 0.15 \text{ ms}$ that corresponds to $\epsilon_a = 0.045 \text{ m}^2 \text{ s}^{-2}$], which propagate through Eq. (3) to be errors in $\Delta\Phi_{4000}^{100}$; and 2) the scatter of the fit of Eq. (3) (see Fig. 1, $\epsilon_b = 0.42 \text{ m}^2 \text{ s}^{-2}$). Biases in the final calibrated $\Delta\Phi_{4000}^{100}$ from this method come from two sources: 1) the error in the measured pressure [0.5 db (R. Wearn 1996, personal communication) that corresponds to about $\epsilon_f = 0.19 \text{ m}^2 \text{ s}^{-2}$], which results in errors in the \mathcal{A} and \mathcal{B} ; and 2) the error introduced in converting the measured τ_{meas} values into τ_{com} ($\epsilon_g = 0.27 \text{ m}^2 \text{ s}^{-2}$), which comes from the scatter in fitting the \mathcal{A} and \mathcal{B} versus pressure curves. An estimate of the total error using this method of calibration, denoted ϵ_{pm} , is given by

$$\begin{aligned} \epsilon_{\text{pm}} &= [(\epsilon_a)^2 + (\epsilon_b)^2 + (\epsilon_f)^2 + (\epsilon_g)^2]^{1/2} \\ &= 0.52 \text{ m}^2 \text{ s}^{-2} \end{aligned}$$

for a wide range of choices of P_{com} (2000–5000 db).

5. Comparison of the two calibration methods

From August 1993 until June 1995, four PIES were deployed in a line across the North Atlantic Current near 42°N (Tracey et al. 1996). During the period of deployment, one to three full-water-column CTDs were taken at each PIES site. Each CTD was used to determine a B' intercept [via Eq. (4)] for determining $\Delta\Phi_{4000}^{100}$ from τ_{meas} , and the τ_{meas} records were calibrated in the traditional manner described in section 3. These same τ_{meas} records were also calibrated using the pressure method described above, and the results of the two calibration methods were compared.

Figure 3 shows the mean of the 22-month time series of $\Delta\Phi_{4000}^{100}$ from each of the four PIES calibrated using the pressure method (circles) and using the traditional method (crosses). The one standard deviation errors are shown for each method. Note that these standard deviations represent only the sources of error that are in-

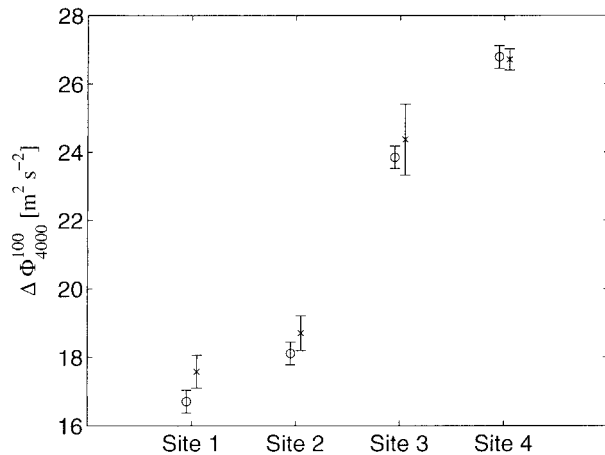


FIG. 3. Plot of the mean of the 22-month time series of $\Delta\Phi_{4000}^{100}$ calibrated via the two different methods. The circles denote the mean from the time series calibrated via the pressure method, and the crosses denote the mean from the traditional calibration method. Error bars denote a one standard deviation error for each method.

dependent between the two methods. Both of the methods for obtaining calibrated $\Delta\Phi_{4000}^{100}$ are impacted in the same manner by the error due to the individual measurements of the τ_{meas} time series and by the error due to the scatter in Eq. (3). Thus, these two error sources are not included in the error bars shown in Fig. 3. The remaining sources of error are all biases, so the error bars would be the same for an individual day as they are for the 22-month averages shown in Fig. 3.

The error bars indicate that the $\Delta\Phi_{4000}^{100}$ time series calibrated using the two different methods are not statistically different. The pressure-calibrated travel times agree with those calibrated by the traditional method to within about $0.47 \text{ m}^2 \text{ s}^{-2}$, which is about 4% of the total North Atlantic Current signal in this region.

6. Summary

The addition of a pressure sensor to the IES has permitted the development of a new method of calibrating a time series of measured acoustic travel times into other dynamic variables without the need for coincident XBTs or CTDs at the IES site during the deployment. Instead, the method relies on the combination of historical hydrography from the region and the measurement of the pressure sensor.

One advantage of calibrating the PIES using the pressure method is that there is a smaller error inherent in the calibration. During the North Atlantic Current experiment the pressure method had a standard deviation in $\Delta\Phi_{4000}^{100}$ of $0.52 \text{ m}^2 \text{ s}^{-2}$, while the traditional method had a standard deviation of $0.65 \text{ m}^2 \text{ s}^{-2}$. The majority ($0.42 \text{ m}^2 \text{ s}^{-2}$) of these errors are due to the rms scatter of the linear relationship between τ and $\Delta\Phi_{4000}^{100}$, which is smaller by as much as a factor of 2 in other ocean regions with tighter temperature–salinity relationships

(such as the Gulf Stream). The scatter about the fitted curve could be reduced by using a curved functional relationship between $\Delta\Phi_{4000}^{100}$ and τ ; however, the improvement would apply to both calibration methods equally. Hence, for the simple purpose of demonstrating the improved accuracy of the pressure method of calibration, a linear fit is adequate.

A second advantage to the pressure method is the elimination of the need for coincident CTDs or XBTs, which reduces the cost and logistical efforts during deployment and recovery. Of course, the bottom pressure record is valuable in its own right to measure the barotropic pressure field (particularly if leveled by combination with deep current measurements), as shown in Shay et al. (1995), Howden (1996), and Lindstrom et al. (1997).

Acknowledgments. The authors would like to express their appreciation to Karen Tracey for her assistance in processing the PIES data and in the preparation of this manuscript. Thanks also to Dr. Allyn Clarke and his colleagues at the Bedford Institute of Oceanography and Dr. Peter Koltermann at the German Hydrographic Service for providing some of the CTD data used in this project. Richard Wearn at ParoScientific, Inc., provided much useful information about the pressure sensors. The reviewers provided a number of useful comments, and our thanks go out to them. Finally, our thanks go out to the crews of the R/V *Oceanus* and CSS *Hudson* for their help in deploying and recovering these instruments. This project was funded under NOAA Grant NA56GP0134 and ONR Contract N00014-92-J-4013.

APPENDIX A

Inherent Offsets in the PIES

Both the pressure and the travel-time measurements made by the PIES are subject to known constant offsets that must be removed prior to calibrating the travel times, as discussed in this paper. The pressure sensors discussed here measure absolute pressure, consisting of the pressure of the ocean plus the pressure of the overlying atmosphere. To combine with the PIES measurement of the acoustic travel time to the sea surface, it is necessary to subtract the atmospheric pressure from the measured pressures. Variations of the mean regional atmospheric pressure from one year to the next are less than 0.1 db, so it is adequate to subtract the annual mean regional atmospheric pressure value rather than to account for the mean over the specific 22-month time period of the experiment. Another offset originates because the acoustic transducer on the PIES is located 0.58 m above the pressure sensor. For combination with the travel time, the corresponding 0.6-db hydrostatic offset was subtracted from the measured pressure. Finally, the IES echo detector has a 3-ms internal response delay in detecting the returning sound pulse. This travel-

time delay must be subtracted from the measured travel times to avoid overestimating the depth, and therefore the pressure, of the IES. (This delay has no effect on the traditional method of calibration because all bias errors are combined into the B' determined from the concurrent CTDs or XBTs.)

APPENDIX B

Projecting τ onto a Common Pressure Level

Simulations using historical hydrography have shown that τ at any one pressure level, P_1 , considerably below the thermocline is linearly related to τ at any other deep pressure level, P_2 :

$$\tau_{P_1} = \mathcal{A} \times \tau_{P_2} + \mathcal{B}. \tag{B1}$$

Examples are shown in Fig. 2. Because variations in τ are on the order of a few milliseconds, while the absolute value of τ is typically a few seconds, errors are minimized in fitting these linear relationships if a large value is subtracted from τ to avoid numerical error. We simply subtracted a constant for each depth, which is the round-trip travel time that would be measured at a given pressure if the ocean had a constant sound speed of 1500 m s^{-1} , τ_{ms} :

$$\tau_{\text{ms}}(P) = \frac{2P}{1500 \text{ ms}^{-1}} \left(\frac{1 \text{ m}}{1.017 \text{ db}} \right) = \left(\frac{2P}{1525.5 \text{ db s}^{-1}} \right), \tag{B2}$$

where the constant 1.017 converts (adequately for this purpose) between pressure and depth. Defining

$$\tau' \equiv \tau - \tau_{\text{ms}},$$

then Eq. (B1) becomes

$$\tau'_{P_1} = \mathcal{A} \times \tau'_{P_2} + \mathcal{B}'. \tag{B3}$$

Simulations of τ' at a number of depths have demonstrated that slopes \mathcal{A} and intercepts \mathcal{B}' of these linear relations are functions of pressure. Thus, a slope, $\mathcal{A}(P)$, and an intercept, $\mathcal{B}'(P)$, can be determined using the pressure measured by each PIES, P_{ies} . Figure B1 shows the slopes and intercepts obtained for converting τ'_{meas} at depths between 2000 and 5000 db into τ'_{com} at 2000 db. Cubic polynomials were fit to \mathcal{A} and \mathcal{B}' as shown. Below 3750 db the coefficient \mathcal{A} was set to a constant value because the error bars at deeper levels grew as the number of CTDs decreased, and the estimates were all consistent with a constant value.

Using \mathcal{A} and \mathcal{B}' and Eq. (B2), the travel times measured by the PIES can be projected into travel times on a single common pressure surface P_{com} . Equation (B3) becomes

$$\tau'_{P_{\text{com}}} = \mathcal{A} \times \tau'_{P_{\text{ies}}} + \mathcal{B}',$$

where $\mathcal{A} = \mathcal{A}(P_{\text{ies}})$ and $\mathcal{B}' = \mathcal{B}'(P_{\text{ies}})$. With each of the individual PIES, τ' records projected onto $\tau'_{P_{\text{com}}}$ it is

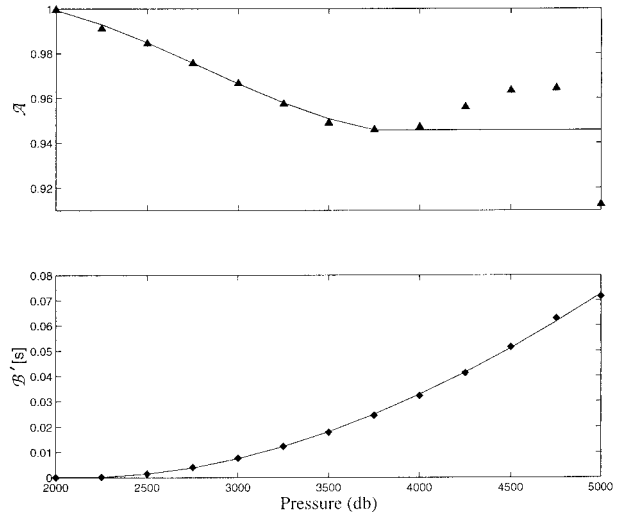


FIG. B1. Slope \mathcal{A} and intercept \mathcal{B}' vs pressure. Symbols show values determined from linear fits to Eq. (B3), with $P_1 = 2000$ db and P_2 along the x axis. Solid lines are cubic polynomial fits to \mathcal{A} and \mathcal{B}' vs pressure. Below 3750 db the coefficient \mathcal{A} was set to a constant value because the observed structure had no physical meaning and was believed to be due to the decreasing number of CTD casts reaching those great depths.

necessary to develop only one set of coefficients, such as A and B of Eq. (3), to convert a τ' time series from any depth into a time series of $\Delta\Phi_{4000}^{100}$ (or into a heat content or potential energy anomaly). The choice of the common pressure level, P_{com} , is arbitrary as long as the level chosen is significantly below the main thermocline.

Another interesting piece of information can be gleaned from Fig. B1. Note that \mathcal{A} varies on the order of 5%. Since the slope between τ' simulated at two different pressure levels is not equal to 1, it can be seen that the historically used assumption that A [in Eq. (3)] was independent of depth could have lead to errors of several percent in $\Delta\Phi_{4000}^{100}$ using the earlier calibration procedures.

REFERENCES

Chaplin, G. F., and D. R. Watts, 1984: Inverted echo sounder development. *IEEE Ocean '84 Conf. Record*, Washington, DC, IEEE, 249–253.

Chiswell, S. M., 1994: Using an array of inverted echo sounders to measure dynamic height and geostrophic current in the North Pacific subtropical gyre. *J. Atmos. Oceanic Technol.*, **11**, 1420–1424.

—, D. R. Watts, and M. Wimbush, 1986: Using inverted echo sounders to measure dynamic height in the eastern equatorial Pacific during the 1982–83 El Niño. *Deep-Sea Res.*, **33**, 981–991.

Fofonoff, N. P., and R. C. Millard, 1983: Algorithms for computation of fundamental properties of seawater. UNESCO Tech. Papers in Marine Science 44, 53 pp.

Garzoli, S. L., and A. Bianchi, 1987: Time–space variability of the local dynamics of the Malvinas–Brazil confluence as revealed by inverted echo sounders. *J. Geophys. Res.*, **92**, 1914–1922.

- , and A. L. Gordon, 1996: Origins and variability of the Benguela current. *J. Geophys. Res.*, **101**, 897–906.
- Hallock, Z. R., 1987: Regional characteristics for interpreting Inverted Echo Sounder (IES) observations. *J. Atmos. Oceanic Technol.*, **4**, 298–304.
- He, Y., D. R. Watts, and K. L. Tracey, 1998: Determining geostrophic velocity shear profiles with IESs. *J. Geophys. Res.*, **103** (3), 5607–5622.
- Howden, S. D., 1996: Processes associated with steep meander development in the Gulf Stream near 68°W. Ph.D. thesis, University of Rhode Island, 229 pp.
- James, C. E., and M. Wimbush, 1995: Inferring dynamic height variations from acoustic travel time in the Pacific Ocean. *J. Oceanogr.*, **51**, 553–569.
- Lindstrom, S. S., X. Qian, and D. R. Watts, 1997: Vertical motion in the Gulf Stream and its relation to meanders. *J. Geophys. Res.*, **102**, 8485–8503.
- Meinen, C. S., and D. R. Watts, 1997: Further evidence that the sound-speed algorithm of Del Grosso is more accurate than that of Chen and Millero. *J. Acoust. Soc. Amer.*, **102**, 2058–2062.
- Qian, X., and D. R. Watts, 1992: The SYNOP experiment: Bottom pressure maps for the Central Array, May 1988 to August 1990. Graduate School of Oceanography Tech. Rep. 3, University of Rhode Island, Narragansett, Rhode Island, 189 pp. [Available from Physical Oceanography Dept., Graduate School of Oceanography, University of Rhode Island, Narragansett, RI 02882.]
- Rosby, T., 1969: On monitoring depth variations of the main thermocline acoustically. *J. Geophys. Res.*, **74**, 5542–5546.
- Shay, T. J., J. M. Bane, D. R. Watts, and K. L. Tracey, 1995: Gulf Stream flow field and events near 68°W. *J. Geophys. Res.*, **100**, 22 565–22 589.
- Tracey, K. L., C. S. Meinen, and D. R. Watts, 1996: North Atlantic Current inverted echo sounder data report for August 1993–July 1995. Graduate School of Oceanography, Tech. Rep. 7, University of Rhode Island, Narragansett, Rhode Island, 54 pp. [Available from Physical Oceanography Dept., Graduate School of Oceanography, University of Rhode Island, Narragansett, RI 02882.]
- , S. D. Howden, and D. R. Watts, 1997: IES calibration and mapping procedures. *J. Atmos. Oceanic Technol.*, **14**, 1483–1493.
- Trivers, G., and M. Wimbush, 1994: Using acoustic travel time to determine dynamic height variations in the North Atlantic Ocean. *J. Atmos. Oceanic Technol.*, **11**, 1309–1316.
- Watts, D. R., and H. T. Rossby, 1977: Measuring dynamic heights with inverted echo sounders: Results from MODE. *J. Phys. Oceanogr.*, **7**, 345–358.
- , and W. E. Johns, 1982: Gulf Stream meanders: Observations on propagation and growth. *J. Geophys. Res.*, **87**, 9467–9476.
- , and H. Kontoyiannis, 1990: Deep-ocean bottom pressure measurement: Drift removal and performance. *J. Atmos. Oceanic Technol.*, **7**, 296–306.
- , K. L. Tracey, J. M. Bane, and T. J. Shay, 1995: Gulf Stream path and thermocline structure near 74°W and 68°W. *J. Geophys. Res.*, **100**, 18 291–18 312.